Available online at www.sciencedirect.com
ScienceDirect
Polymer 48 (2007) 2958–2968
polymer
www.elsevier.com/locate/polymer

Effect of temperature and strain rate on the tensile deformation of polyamide 6

Gui-Fang Shan, Wei Yang*, Ming-bo Yang*, Bang-hu Xie, Jian-min Feng, Qiang Fu

College of Polymer Science and Engineering, Sichuan University, State Key Laboratory of Polymer Materials Engineering, Chengdu, 610065 Sichuan, People's Republic of China

Received 2 October 2006; received in revised form 9 February 2007; accepted 6 March 2007
Available online 12 March 2007

Abstract

The effects of the draw temperature and the strain rate on the tensile deformation of polyamide 6 (PA6) were investigated using three PA6 samples with different initial shapes and physical dimensions. It is observed that the special double yielding phenomenon is indeed present in PA6, provided that certain temperature and strain rate are given, as well as the appropriate initial structure. The results also show that the dependence of the first yield stress on temperature is nearly linear while on strain-rate is logarithmic. The temperature and strain-rate sensitivity change at the draw temperature in the vicinity of the glass transition temperature of PA6. The double yielding of PA6 is not only the combination of two thermally activated rate processes depending on temperature and strain rate, but also associated with the initial structure of samples. The yielding manner for PA6 seems to be determined by the synergetic effect of both the deformation of amorphous and crystalline phases. Thus some special structure involving the crystalline and amorphous phases should come into being in PA6 exhibiting double yielding. Especially the important role of inter- and intra-link should be taken into account. The theory of partial melting–recrystallization cannot account fully for the double yielding of PA6.
© 2007 Elsevier Ltd. All rights reserved.

Keywords: Draw temperature; Strain rate; Double yield

1. Introduction

The study of the tensile deformation behavior of polymeric materials has been the subject of numerous investigations in a number of previous publications and the extensive work has established that both the draw temperature and the strain rate are the crucial factors in determining the deformation characteristics of polymers [1–13]. It is well known that the Eyring formalization [1] for thermally activated rate processes has been the most largely used model for clarifying the yield mechanism of glassy and semicrystalline polymers. A detailed investigation of the yielding behavior of poly(methyl methacrylate) (PMMA) and polycarbonate (PC) over a wide range of strain rates and temperatures by Roetling [3] and Bauwens [4] has shown that the yield stress increases rapidly with increasing strain rate and decreasing temperature at low temperatures and high strain rates than at high temperatures and low strain rates. Therefore, it has been proposed that the Eyring equation can be extended, under the assumption that there is more than one activated rate process, the stresses being additive. Vinogradov et al. [5,6] have dealt with the tensile flow and stress–strain behavior of poly(butyl methacrylate) at different testing conditions and found that: (1) over broad ranges of stresses and strain rates such polymers behave as linear viscoelastic bodies and the peculiar deformation properties are due to transitions from the fluid to rubbery, leathery, and glassy states as stress- and strain-rate increase; (2) its dependence on the stress is exponential in the temperature range below T_g, whereas at temperature above T_g a power law fits the data. Most recently, Mahieux and Reifsnider [7] have put forward a statistical model to describe the stiffness variation of polymers over

* Corresponding authors. Tel./fax: +86 28 8546 0130.
E-mail addresses: ysjsanjin@163.com (W. Yang), yangmb@scu.edu.cn (M.-b. Yang).

0032-3861/$ - see front matter © 2007 Elsevier Ltd. All rights reserved.
doi:10.1016/j.polymer.2007.03.013

a wide range of temperatures. Also, starting from the consideration of strain-rate dependence of the stiffness, Richeton et al. [8] have proposed a robust physically based model for predicting the stiffness for a wide range of temperatures and strain rates. Additionally, much attention has been focussed on the effect of temperature as well as strain rate on the tensile behavior of thermoplastic matrix composites. The results from Mallick and associates [9] have revealed that short fiber reinforced polyamide 6 (PA6) composite is a strain rate and temperature dependent material. The strain rate and temperature sensitivity differ at a temperature between 25 °C and 50 °C as a result of the glass transition of the PA6 matrix.

In particular, Seguela and co-workers [10,11] have made a comprehensive researches on the yielding behavior of medium density polyethylene (MDPE) and drawn the conclusion that the yielding process of MDPE involves two thermally activated rate processes operating cooperatively, but having different activation parameters relative to both temperature and strain rate. It has been pointed out that PEs which give rise to a sharp yield point at room temperature may display a double yield point at higher draw temperature. Subsequently, they have paid special attention to studying the yielding behavior of PE and related copolymers and found that either homogeneous or heterogeneous deformation under tensile testing should be in existence in PEs. The stronger thermal activation of homogeneous slip makes it become more favorable than heterogeneous slip as temperature increases and strain rate slows down. However, the heterogeneous slip may be activated as deformation proceeds owing to its lower strain hardening [12]. In the past two decades, various investigations have been carried out in order to gain a better insight into the double yielding of PEs and some valuable results and models can be available [10–18].

The occurrence of double yielding in PA6 films, carefully dried under vacuum, was first recognised by Hoashi et al. [19] without any comments. However, to the best of the authors' knowledge, no extra literatures were reported concerning this special phenomenon of PA6 after that, except our recent publications [20–23]. A qualitative analysis about the effect of temperature and strain rate on tensile deformation including the double yielding of PA6 is provided in present paper, and the origin of double yielding of PA6 will be discussed in more detail in subsequent reports.

2. Experimental procedure

2.1. Material

The polyamide 6 (PA6) resin used here was a commercial product of Xinhui Meida-DSM Nylon Slice Company LTD., supplied in pellets, with the trade mark M2800, as described previously [20–23]. The melt flow rate (MFR) of the resin is 4.09 g/10 min at 275 °C, exerting a force of 325 g. The resin was dried for 12 h under vacuum at 100 °C before injection molding to avoid its hydrolytic degradation.

2.2. Sample preparation and tensile measurement

The strictly dried PA6 resin was injection molded into dog-bone specimens using an injection molding machine PS40E5ASE made in Nissan, Japan, with a temperature profile of 230 °C, 240 °C, 250 °C, and 245 °C from the feeding zone to the nozzle. In order to account for the dependency of temperature and strain rate on the tensile deformation of plain PA6, a series of samples with different shapes and dimensions were prepared, as schematically illustrated in Fig. 1. For the sake of briefness, hereafter, these samples are referred to as A, B and C. Accordingly, the injection molding parameters were not identical for different samples. The injection velocity of 14% and 32% (the maximal injection velocity is 45 g/s) was adopted for the thickest (sample A) and the thinnest (sample C) samples, respectively. The injection pressure of 30% and 38% (the maximal injection pressure is about 187 MPa) was employed, respectively. The mold temperature of 70 °C was utilized only for the thinnest sample C.

The testing in tension was carried out using dumbbell-shaped samples over a range of draw temperatures and strain rates. The samples were kept in oven of the Instron tensile testing machine at the definite temperature of the drawing experiment for about 5 min prior to drawing. The distance between the grippers was 50 mm for sample A and 25 mm for samples B and C. At least five samples were used for each measurement and the average results were reported here. The nominal stress and nominal strain are defined as the ratio of the draw force to the initial cross-section of samples and the ratio of the crosshead displacement to the initial gauge length of samples, respectively. The nominal strain rate is the ratio of the crosshead speed to the initial gauge length of the sample.

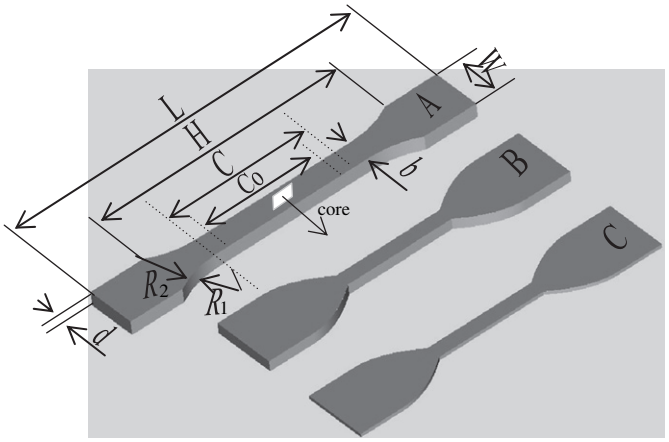

Fig. 1. Schematic representation for injection molding specimens in the present study (unit: mm). Sample A: $L = 154$, $H = 110$, $C = 55 \pm 0.5$, $C_0 = 50 \pm 0.5$, $W = 20 \pm 0.2$, $b = 10 \pm 0.2$, $d = 4.26 \pm 0.02$, $R_1 = R_2 = 75$; sample B: $L = 110$, $H = 76$, $C = 26 \pm 0.5$, $C_0 = 25 \pm 0.2$, $W = 25$, $b = 6.5 \pm 0.1$, $d = 3.42 \pm 0.02$, $R_1 = 14$, $R_2 = 25$; sample C: $L = 110$, $H = 76$, $C = 26 \pm 0.5$, $C_0 = 25 \pm 0.2$, $W = 25$, $b = 6.5 \pm 0.1$, $d = 1.40 \pm 0.02$, $R_1 = 14$, $R_2 = 25$.

2.3. Characterization

The materials of 5 mg or so taken from the core layer at the intermediate position of samples, depicted in Fig. 1, were studied by means of a Netzsch DSC-204 differential scanning calorimeter from 0 °C to 250 °C at a scanning rate of 10 °C/min with 50 mL/min N_2 protection. The melting of indium and zinc samples was used to calibrate the temperature and the heat-flow scales at the same heating rate. The weight fraction crystallinity can be assessed based on Eq. (1):

$$X_c(\%) = \frac{\Delta H_f}{\Delta H_f^0} \times 100 \tag{1}$$

where ΔH_f is the enthalpy of fusion of samples and ΔH_f^0 is the extrapolated value of the enthalpy corresponding to the melting of 100% perfect infinite crystalline sample. Two main crystals of α- and γ-form of pure PA6 are usually observed in most cases and for this reason an average value of 190 J/g has been chosen for ΔH_f^0 [24,25].

A wide-angle X-ray diffraction measurement was carried out with a Philips X'Pert Graphics & Identify instrument (The Netherlands) at room temperature to determine crystal parameters and crystallinity indices of samples. The materials were also taken from the core layer at the intermediate position of samples. The Cu Kα irradiation source was operated at 50 kV and 30 mA and the diffraction patterns were recorded with a step size of 0.02° from $2\theta = 5°$ to 40°. The center of the broad peak on each X-ray pattern was attributed to the average chain distance of polyamide chains. The d spacing is calculated by substituting the scattering angles of the peak into the Bragg's equation [26], namely:

$$d_{hkl} = \frac{\lambda}{2\sin\theta} \tag{2}$$

where, θ is the X-ray diffraction angle and wave length $\lambda = 1.54056$ Å.

Following the work of Gurato et al. [24], the XRD curve of PA6 can be deconvoluted into five components by approximating the peaks with Gaussian curves. The five components consist of $(020)_\gamma$, $(200)_\gamma$, $(200)_\alpha$, and $(002)_\alpha$ diffraction peaks appearing at about $2\theta = 11.0°$, 21.9°, 20.4°, and 24.0°, respectively, and a broad peak due to the amorphous phase. The crystallite dimension H_{hkl} perpendicular to the plane hkl and the crystallinity indices CI (%) could be determined as follows:

$$H_{hkl} = \frac{K\lambda}{\beta\cos\theta} = \frac{K\lambda}{\sqrt{F_{whm}^2 - b_0^2} \times \frac{\pi}{180} \times \cos\theta} = \frac{0.89 \times 1.54056}{\sqrt{F_{whm}^2 - 0.15^2} \times \frac{\pi}{180} \times \cos\theta} \tag{3}$$

$$CI_\alpha(\%) = \frac{\sum A_{\alpha\text{-form crystal}}}{\sum\left(A_{\alpha\text{-form crystal}} + A_{\gamma\text{-form crystal}}\right) + A_{\beta\text{-form}}} \times 100$$

$$CI_\gamma(\%) = \frac{\sum A_{\gamma\text{-form crystal}}}{\sum\left(A_{\alpha\text{-form crystal}} + A_{\gamma\text{-form crystal}}\right) + A_{\beta\text{-form}}} \times 100$$

$$CI_{total}(\%) = \frac{\sum\left(A_{\alpha\text{-form crystal}} + A_{\gamma\text{-form crystal}}\right)}{\sum\left(A_{\alpha\text{-form crystal}} + A_{\gamma\text{-form crystal}}\right) + A_{\beta\text{-form}}} \times 100 \tag{4}$$

where, K is the constant assigned 0.89 in our study; β is the integral breadth or breadth at half-maximum intensity; b_0 is the broaden factor of the apparatus and F_{whm} is the half-diffraction peak width; $A_{\alpha\text{-form}}$ and $A_{\gamma\text{-form}}$ are the areas under the α- and γ-form crystal peaks, respectively; $A_{\beta\text{-form}}$ is the area under the broad peak due to the amorphous phase.

The dynamic mechanical analysis was performed on the instrument DMA Q800 using clamp single cantilever mode with a frequency of 1 Hz. The scanning temperature ranged from −140 °C to 160 °C at a heating rate of 3 °C/min. For the low temperature relaxations, liquid nitrogen was used at atmospheric pressure and the β- and α-relaxation (T_g) of PA6 were collected from the transition peak maxima in dynamic loss moduli or damping tan δ.

3. Results and discussion

3.1. Temperature and strain-rate dependence

Fig. 2 illustrates the nominal stress–strain curves of plain PA6 for sample A as a function of draw temperature at different strain rates. The crosshead speeds of apparatus were set at 1 mm/min, 5 mm/min, 10 mm/min and 50 mm/min. According to the definition of nominal strain rate above, it can be calculated that the corresponding nominal strain rates were $0.33 \times 10^{-3}\ s^{-1}$, $1.67 \times 10^{-3}\ s^{-1}$, $3.33 \times 10^{-3}\ s^{-1}$ and $1.67 \times 10^{-2}\ s^{-1}$. First we consider the influence of the temperature. On the whole, the sample exhibits a predominant initial single yield point, Y_1, at low temperature but with temperature increasing a broader second yield point, Y_2, is observed, as the arrows labelled in Fig. 2(a). However, as the temperature reaches a certain level, the stress–strain curves only display a very broad plateau region without evident local maximum, similar to the rubber-like deformation. As for the influence of the strain rate, it is obvious that the double yielding phenomenon displays easily at relatively lower strain rate. For example, for samples tested at temperature of 15 °C, the apparent double yielding occurs at the strain rate of $0.33 \times 10^{-3}\ s^{-1}$, as illustrated in Fig. 2(a). Comparatively, the yielding is sharp and dominated by a single peak with only a very minor secondary peak at higher strain rates (see Fig. 2(b)–(d)). In other words, the character of yielding varies with respect to both temperature and strain rate. Generally, the double yielding of PA6 is inclined to appear at high temperatures and low strain rates, similar to the results of PEs [13,14]. Again, it should be identified here that two different types of double yielding pattern exist in PA6, as schematically shown in curves A and B in Fig. 2(a). The first stress level is higher than the second one in type A curve while the case in curve B

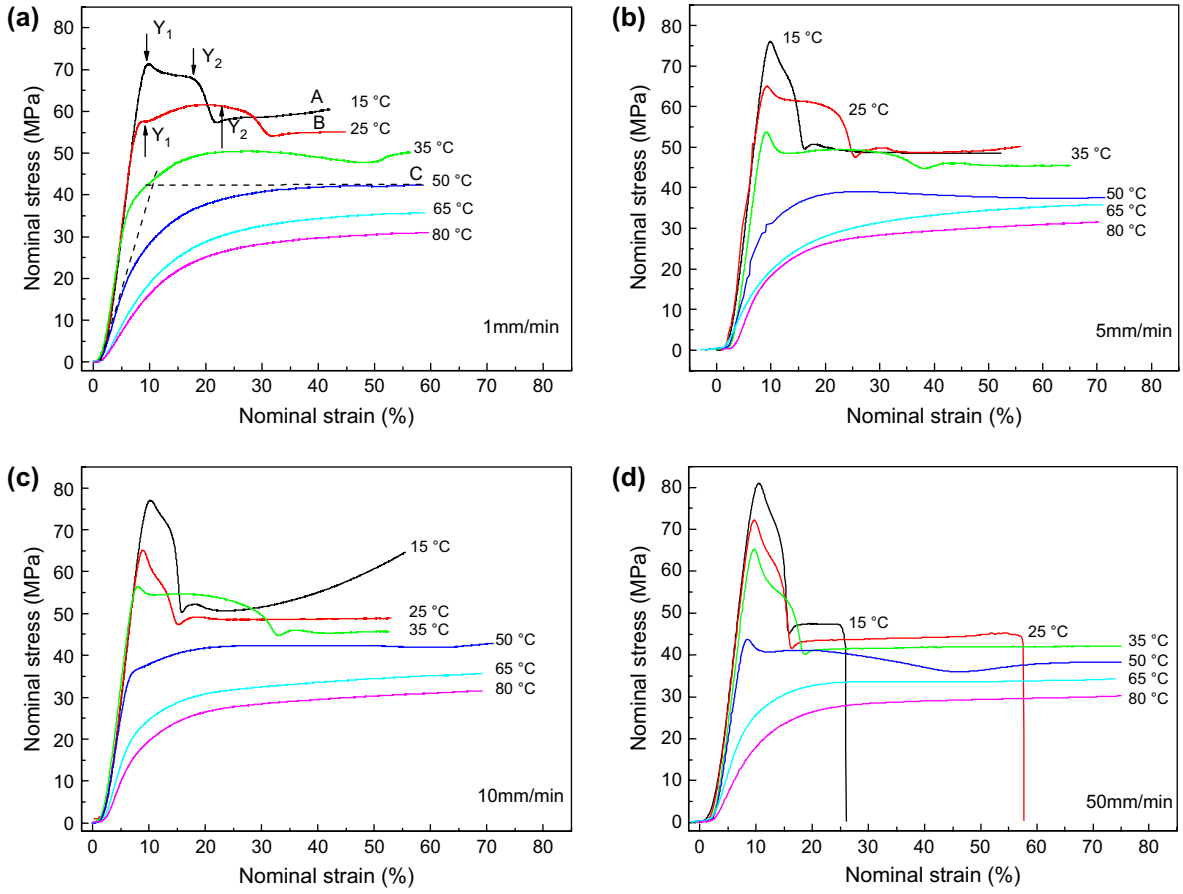

Fig. 2. Nominal stress–strain curves of plain PA6 for sample A as a function of draw temperature for a constant nominal strain rate of (a) $0.33 \times 10^{-3}\ s^{-1}$; (b) $1.67 \times 10^{-3}\ s^{-1}$; (c) $3.33 \times 10^{-3}\ s^{-1}$; (d) $1.67 \times 10^{-2}\ s^{-1}$.

is the other way round. It is deemed here that the higher second yield stress in curve B is resulted from both the further crystallization induced in a uniaxial deformation at a rather low strain rate and the partially melting and recrystallization of less perfect crystallites at relatively high temperature. Accordingly, the further crystallization will be absent in the case of high strain rate, leading to the decrease of the second yield stress. Again, it is not necessary for a large temperature increase to take place in order for partial melting to occur, as the heat is also generated during the drawing process. Thus, the partial melting–recrystallization will be absent if the temperature is higher, resulting in the decrease of the second yield stress similarly.

On the basis of above discussion, a fundamental question is addressed, namely how the temperature and strain rate affect the yielding deformation of polyamide **6**. In our research to understand this issue, the results showing the first yield stress of sample A as a function of both temperature and strain rate are plotted in Fig. 3. Prior to making some comments, it should be mentioned here that how the yield stress is measured in the case of the curves similar to rubber-like pattern. The method used here is based on the intersecting lines from the initial modulus and the almost linear region past the yield point [13], as represented in the curve C of Fig. 2(a). As expected, the first yield stress decreases nearly linearly with increasing temperature and decreasing logarithm of strain rate. However, with the temperature further increasing to higher than 50 °C, the effect of the strain rate on both the shape of stress–strain curves and the first yield stress becomes more and more negligible, as shown in Figs. 2 and 3. Thus, in the case of the temperature below 50 °C, the Eyring equation describing the first yield stress of PA6 can be simplified in the form of Eq. (5):

$$\sigma_y = A + BT \log \varepsilon' \tag{5}$$

3.2. Influence of the geometry dimensions on the tensile deformation

As described above, the occurrence of double yielding of PA6 is dependent on the external testing conditions including the temperature and strain rate. But how about the effect of the initial microstructure formed during the injection molding process? In order to gain more information on this topic and the relation between the double yielding of PA6 and structural factors, the other two samples with different shapes and dimensions were tested at a series of temperatures and strain rates. The crosshead speeds for sample B were set at 1 mm/min, 10 mm/min and 100 mm/min and for sample C

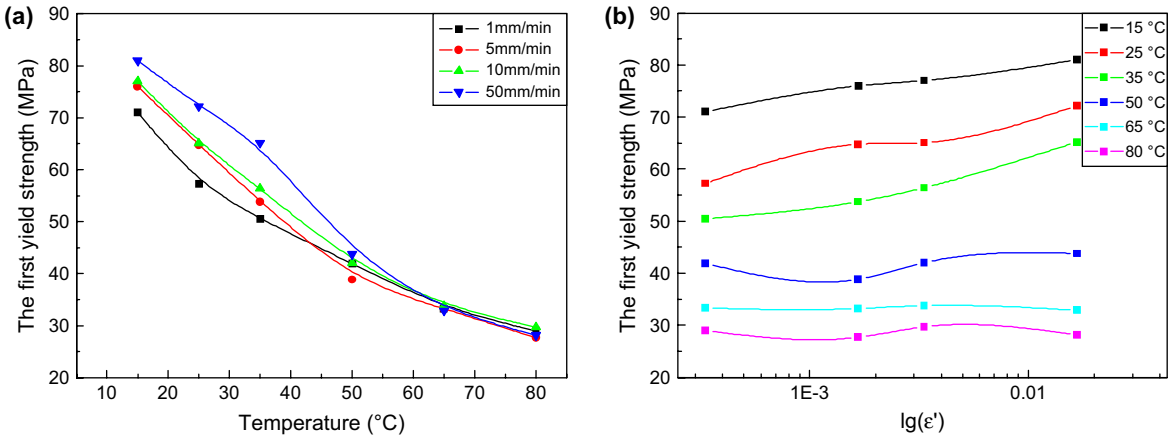

Fig. 3. The first yield stress of sample A as a function of (a) draw temperature at different nominal strain rates and (b) log of strain rate, log ε′, at different draw temperatures.

were 1 mm/min, 5 mm/min, 10 mm/min and 50 mm/min. Since the gauge length for samples B and C was 25 mm, so the nominal strain rates were different from sample A. The corresponding results are given in Figs. 4–7.

Similar to the case of sample A, for samples B and C, depending on the temperature and strain rate, either a single yield or a double yield may occur, as illustrated in Figs. 4 and 6. However, the temperature and strain rate sensitivity for different samples are not identical, namely the parameters A and B in Eq. (5) are different for samples A, B and C. For the sake of clarity, the appearance of double yielding of samples under different testing conditions is summarized in Table 1. Comparatively speaking, the double yielding is inclined to be present in sample A, the thickest one. For sample C, the thinnest one, the double yielding only has taken place at the strain rate below 5 mm/min. In the case of strain rate above 5 mm/min, irrespective of the temperature, only a single yield or a local maximum is observed in sample C. Therefore, we can draw the conclusion that the double yielding of PA6 is not only associated with the testing conditions, namely a combination of two thermally activated rate processes depending on temperature and strain rate, but also has a marked relation to the initial structure formed in sample. Furthermore, the structural evolvement of PA6 films of about 80 μm thick in tensile deformation has been studied in detail by Coulon et al. [27,28] using atomic force microscopic (AFM) analysis and the double yielding was not reported in such films, where some special microstructure cannot come into being for PA6 films exhibiting double yielding because of the thin enough thickness in our opinion, as also approved above conclusion.

Also, the first yield stress of samples B and C varied with temperature and strain rate is shown in Figs. 5 and 7, respectively. The general influence tendency of temperature and strain rate on samples B and C can be explained in a similar manner with sample A, namely the first yield stress decreases with temperature increasing and strain rate decreasing, and the temperature sensitivity or gradient is nearly linear while the strain rate gradient is logarithmic below a certain temperature. In addition, combining with Figs. 2–7, it is evident that increasing thickness of samples will lead to a reduction of tensile yield stress, as is consistent with the results of Uribe-Arocha et al. [29], who have also reported that in the fracture surface of thicker tensile specimens the formation of a sheet-like structure was observed in PA6-clay nanocomposites.

4. Discussion

Based on the extensive set of data generated with diverse PA6 samples we can draw the conclusion that double yielding is indeed in existence in PA6, provided that an appropriate initial structure and testing condition can be achieved. Very distinct changes in the shape of stress–strain curves of PA6 samples can be observed as there dependent variables are altered. The experimental observation has given the direct information evident sharp necking was discerned in the vicinity of the second yield point Y_2, where the permanent plastic deformation may be taken place. In contrast, the first yield point Y_1 is most probably accompanied by the deformation of the amorphous phase of PA6, including the interlamellar sliding or shear, lamellar separation and lamellar cluster rotation in our opinion.

In the following paragraphs we will discuss some differences in initial structure of samples with different thickness by means of DSC, XRD and DMA analyses, including the interplanar distance d_{hkl}, the crystallite dimension H_{hkl}, the quantitative determination of α, γ, and δ (amorphous) phases, the β-relaxation, the α-relaxation at T_g temperature, and so on. Fig. 8 shows the changes of DSC melting curves of samples A, B and C. The results indicate that both the crystal thickness and the perfection of crystallite increase with sample thickness increasing, since the melting temperature of main peak I, characterizing the crystal thickness, has a slight increment with increasing sample thickness. In addition, the melting region is broadened, as well as the area of shoulder peak increases when the sample thickness decreases, roughly indicating the relatively poor crystallite perfection. In order to give more insight into different crystalline planes of samples, the XRD patterns and corresponding deconvolution curves are depicted

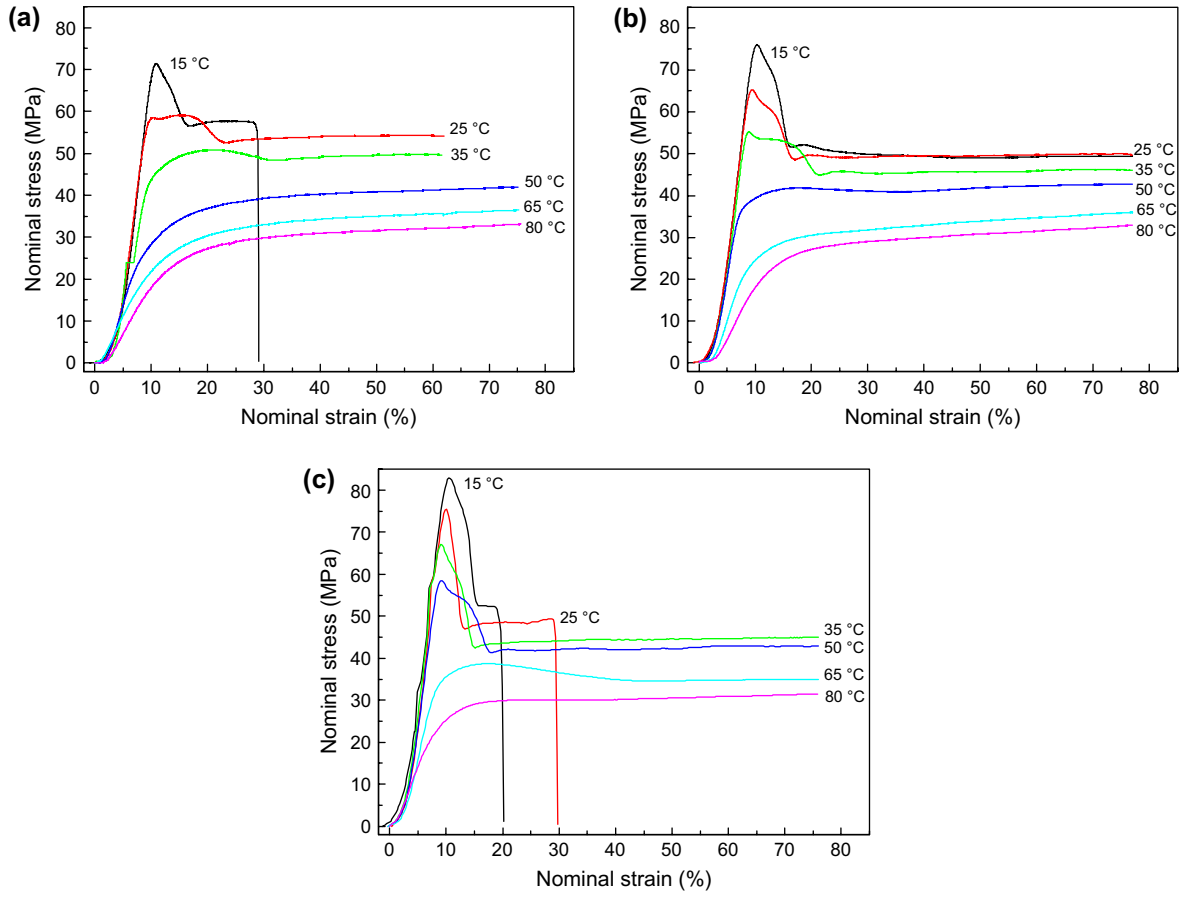

Fig. 4. Nominal stress–strain curves of plain PA6 for sample B as a function of draw temperature for a constant nominal strain rate of (a) $0.67 \times 10^{-3}\ s^{-1}$; (b) $6.67 \times 10^{-3}\ s^{-1}$; (c) $6.67 \times 10^{-2}\ s^{-1}$.

in Figs. 9 and 10, respectively. The calculated values based on Eqs. (2)–(4) are listed in Table 2. According to these results, it seems that the primarily existed crystal form is γ form in sample C, whereas both the α- and γ-form are existed in samples A and B. Moreover, the content of γ form increases from 3.2% to 8.5% for the thickness decreases from 4.26 mm to 3.42 mm. Again, it is found that an increase in the thickness is accompanied by an increase in total core crystallinity from 7.4% to 12.5%. In fact, Akkapeddi [30] has also reported that crystallinity in the core of injection molded PA specimens increased dramatically with sample thickness increasing, while remaining nearly constant in the skin. In agreement with the changes of core crystallinity against sample thickness, the interplanar distance d_{hkl} of both α- and γ-form also increases with the thickness increasing, as well as the crystallite dimension H_{hkl}.

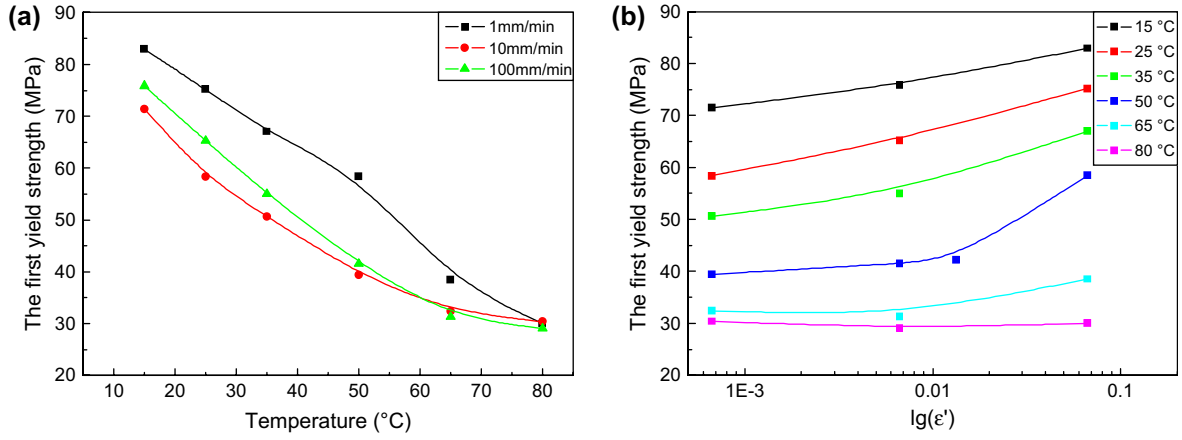

Fig. 5. The first yield stress of sample B as a function of (a) draw temperature at different nominal strain rates and (b) log of strain rate, log ε′, at different draw temperatures.

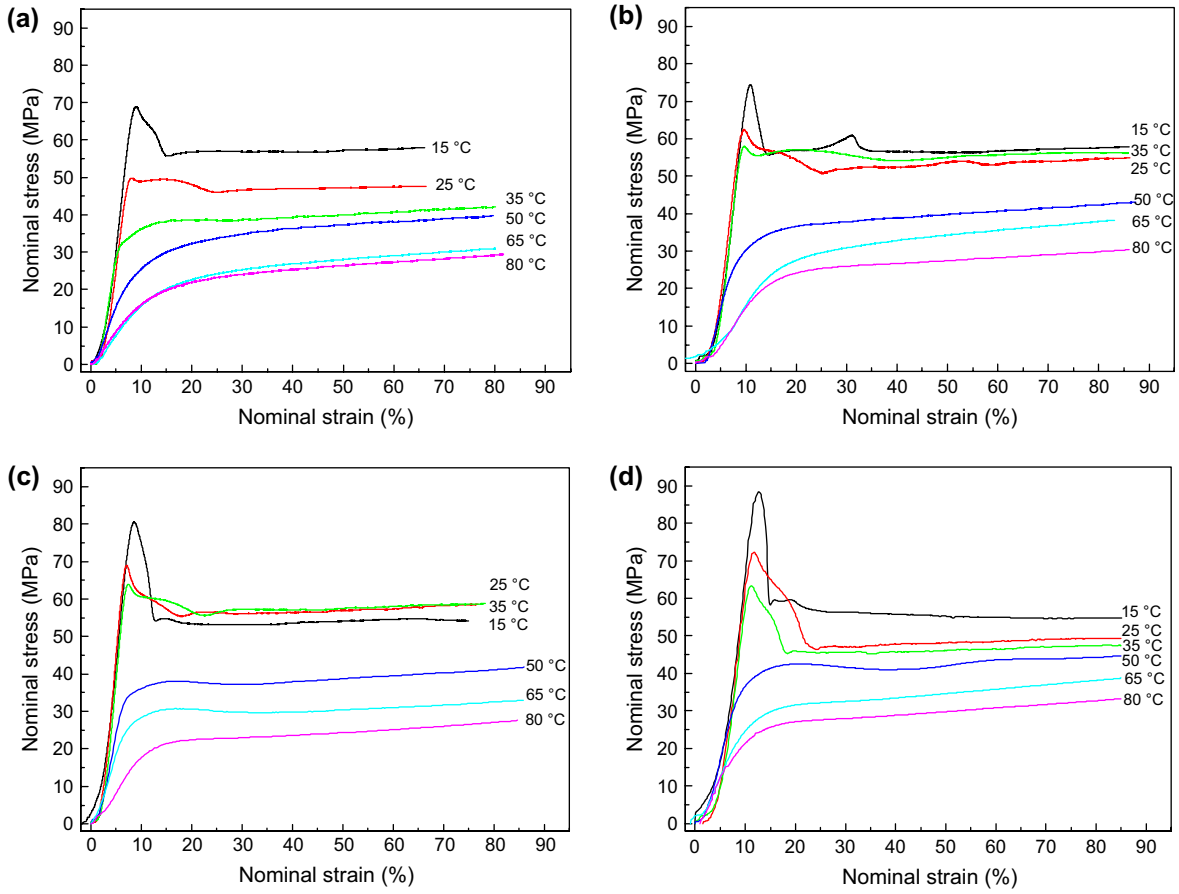

Fig. 6. Nominal stress–strain curves of plain PA6 for sample C as a function of draw temperature for a constant nominal strain rate of (a) $0.67 \times 10^{-3}\ s^{-1}$; (b) $3.33 \times 10^{-3}\ s^{-1}$; (c) $6.67 \times 10^{-3}\ s^{-1}$; (d) $3.33 \times 10^{-2}\ s^{-1}$.

In terms of above discussion, it is notable that the characteristics in crystalline phase vary with the sample thickness significantly. However, the content of amorphous phase of PA6 used in this study exceeds much more than 50%, as shown in Table 2. Thus it is very necessary to consider the structural change of amorphous phase, as will be discussed in the following text. Firstly, the effect of sample thickness on the storage modulus is clearly shown in Fig. 11(a). Thinner samples exhibit higher storage moduli, thus higher stiffness. From the DMA results shown in Fig. 11(b) and (c), it is worth mentioning that besides the obvious primary dissipation, i.e. α-relaxation peak at T_g temperature, there is also a distinct secondary dissipation, i.e. β-relaxation peak at lower temperature. For sample A, the α- and β-relaxation peaks are about

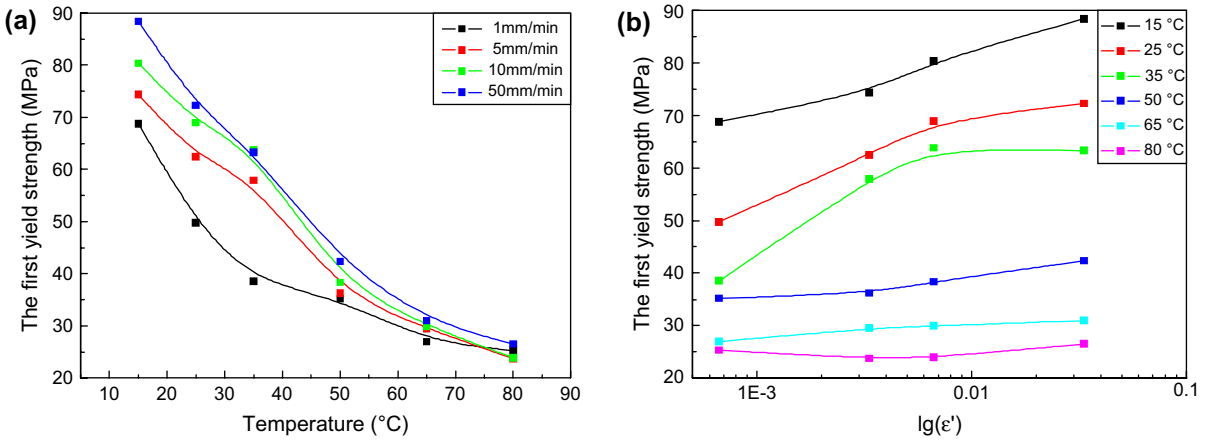

Fig. 7. The first yield stress of sample C as a function of (a) draw temperature at different nominal strain rates and (b) log of strain rate, log ε′, at different draw temperatures.

Table 1
The occurrence of double yielding in PA6 samples under different testing conditions

Sample	Strain rate (mm/min)	Temperature (°C)					
		15	25	35	50	65	80
A	1	✓	✓	×	×	×	×
	5	×	✓	✓	×	×	×
	10	×	×	✓	×	×	×
	50	×	×	×	✓	×	×
B	1	×	✓	×	×	×	×
	10	×	×	✓	×	×	×
	100	×	×	×	✓	×	×
C	1	×	✓	×	×	×	×
	5	×	×	✓	×	×	×
	10	×	×	×	×	×	×
	50	×	×	×	×	×	×

63.45 °C and −54.18 °C, respectively. And the values of 60.07 °C and −55.67 °C for sample B and 51.87 °C and −62.41 °C for sample C are obtained. Together with the tensile deformation results, we can see the temperature and strain rate sensitivity change at the temperature in the vicinity of T_g of PA6. What is of great importance in Fig. 11 is that for sample A, below the α-relaxation peak, there are a broad shoulder peak from 20 °C to 50 °C and a loss modulus plateau from −25 °C to 20 °C. The storage modulus corresponding to this loss modulus plateau increases with scanning temperature increasing, which is contrary to the cases of samples B and C. Generally speaking, the α-transition of PA is related with the breakage of the hydrogen bond network, while the β-transition is mainly due to the movement of the carbonyl group in amorphous phase [31].

In the past, some theories and models were proposed to account for the occurrence of yielding and double yielding [10–14,32–37]. Some researcher employed the local melting–recrystallization theory to explain the double yielding of PEs. During the tensile deformation, the concentration of the stress on less perfect crystallites causes them to partially melt and

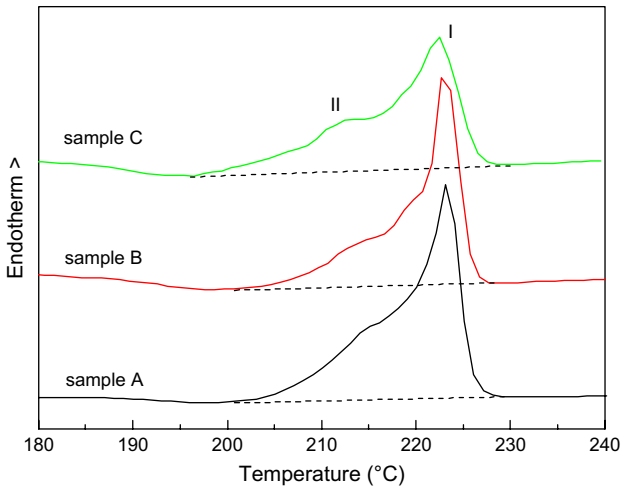

Fig. 8. The DSC melting curves of molded samples A, B and C.

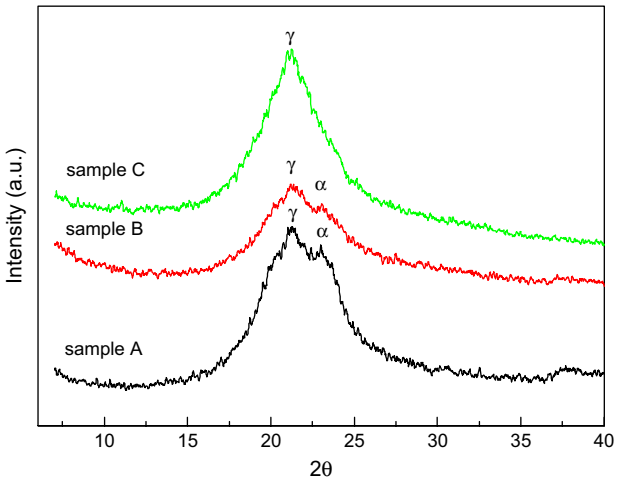

Fig. 9. The X-ray diffraction patterns for samples A, B and C.

recrystallize. Potentially crystallizable materials form a new population of oriented crystallites. Therefore, the two yield points result from the yielding of the original and the new crystallites, respectively [14,33]. However, the local melting–recrystallization theory seems to be not applicable to discuss the double yielding of PA6. The DSC melting curves of drawn sample C experiencing tensile tests at different temperatures and strain rates are shown in Fig. 12 and the corresponding crystallinity based on Eq. (1) is summarized in Table 3. It can be seen that, compared with the undrawn samples shown in Table 2, the crystallinity of drawn sample is relatively much higher, which is likely to be attributed to the stress-induced recrystallization process, although the lamellae will be disrupted during deformation. The higher the strain rate, the more the lamellae will be fragmented. With the temperature increasing, lamellar fragmentation is favored by the more regularly chain folded systems formed at higher draw temperature. Most importantly, an extra shoulder peak II near the main melting peak I appears at higher temperature for sample C tested at lower strain rate and higher temperature, referring to curves (3) and (4) in Fig. 12(a), with the former sample tested at 5 mm/min and 35 °C and the latter at 5 mm/min and 65 °C. The additional peak at higher temperature may be ascribed to the melting of the lamellae recrystallized during the tensile deformation because of the lower strain rate and higher temperature, which provide much more time and activated heat energy for molecular rearrangement to form perfect crystallites or new crystallites. On the other hand, in view of the fact that the double yielding disappears at the strain rate of 5 mm/min and temperature of 65 °C for sample C, as described previously, the theory of local melting–recrystallization is still in question for explaining double yielding of PA6. Perhaps this situation lies in the lack of considering the contribution of the amorphous phase to double yielding [12] with respect to the theory of local-melting recrystallization and an overall consideration on the coupling of the crystalline region with the amorphous one is demanded for solving the deformation mechanism of double yielding of PA6, as well as the role of the inter- and intra-link

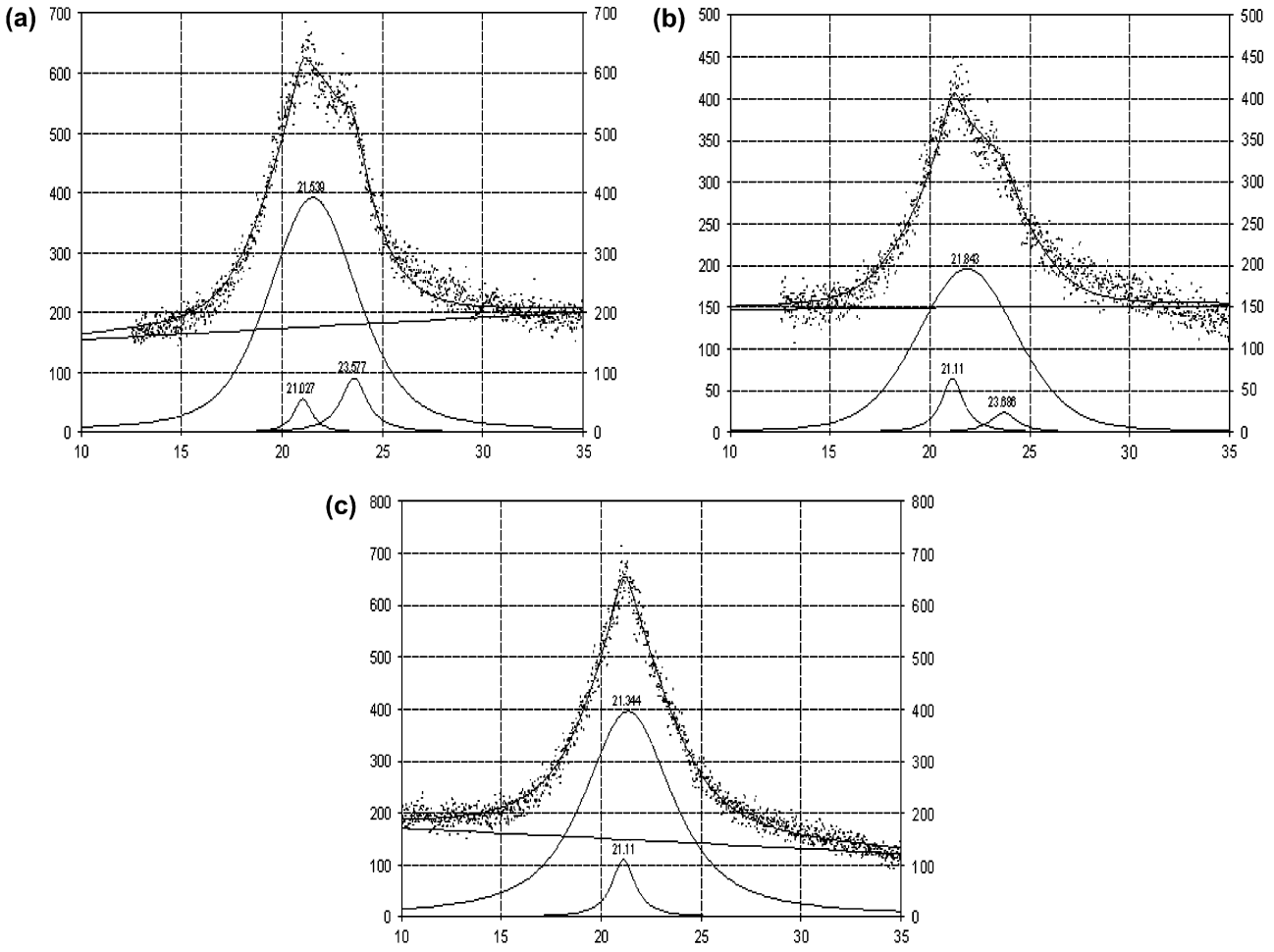

Fig. 10. The deconvolution curves of the X-ray diffraction curve of samples (a) A, (b) B, and (c) C.

[23]. The former is formed by crystallizing one molecule in two different lamellae simultaneously and binds several stacked lamellae, acting as a transmitter of external load, while the latter arises from the intra-lamellar tie molecules [32], depressing the micro-necking process, namely controlling the extent of the second stress plateau region prior to necking in our opinion. For sample A, bringing forth the double yielding relatively frequently, some special microstructure should come into being. From the DSC and XRD results, it is indicated that the crystal thickness, the perfection of crystallite, the core crystallinity, the interplanar distance and the crystallite dimension of sample A are also relatively higher than that of samples B and C. From the DMA result, the occurrence of the shoulder peak in the vicinity of α-relaxation peak for sample A means that some specific structure also formed in amorphous phase, probably related with the formation of a continuous network by tie molecules, responsible for large improvement in yielding behavior. Thus the yielding manner of PA6 seems to be determined by the synergetic effect of both the deformation of amorphous and crystalline phases. Some specific structure involving the crystalline and amorphous phases should come into being in PA6 exhibiting double

Table 2
X-ray diffraction data for the core layer of PA6 injection molded samples

Sample	*hkl*	2θ (°)	FWHM	Area	Amplitude	d_{hkl} (nm)	H_{hkl} (nm)	CI (%)
A	γ_{200}	21.03	1.090	97.76	57.10	0.4221	7.40	3.24
	δ	21.54	5.237	2691.46	392.79	0.4122	1.53	89.16
	α_{002}	23.58	1.590	229.50	91.91	0.3770	5.07	7.60
B	γ_{200}	21.11	1.321	135.61	65.35	0.4205	6.09	8.53
	δ	21.84	5.871	1390.42	196.87	0.4066	1.36	87.51
	α_{002}	23.69	1.658	62.92	24.15	0.3753	4.86	3.96
C	γ_{200}	21.11	1.398	244.77	111.48	0.4205	5.75	7.39
	δ	21.34	5.289	3068.49	396.92	0.4160	1.51	92.61

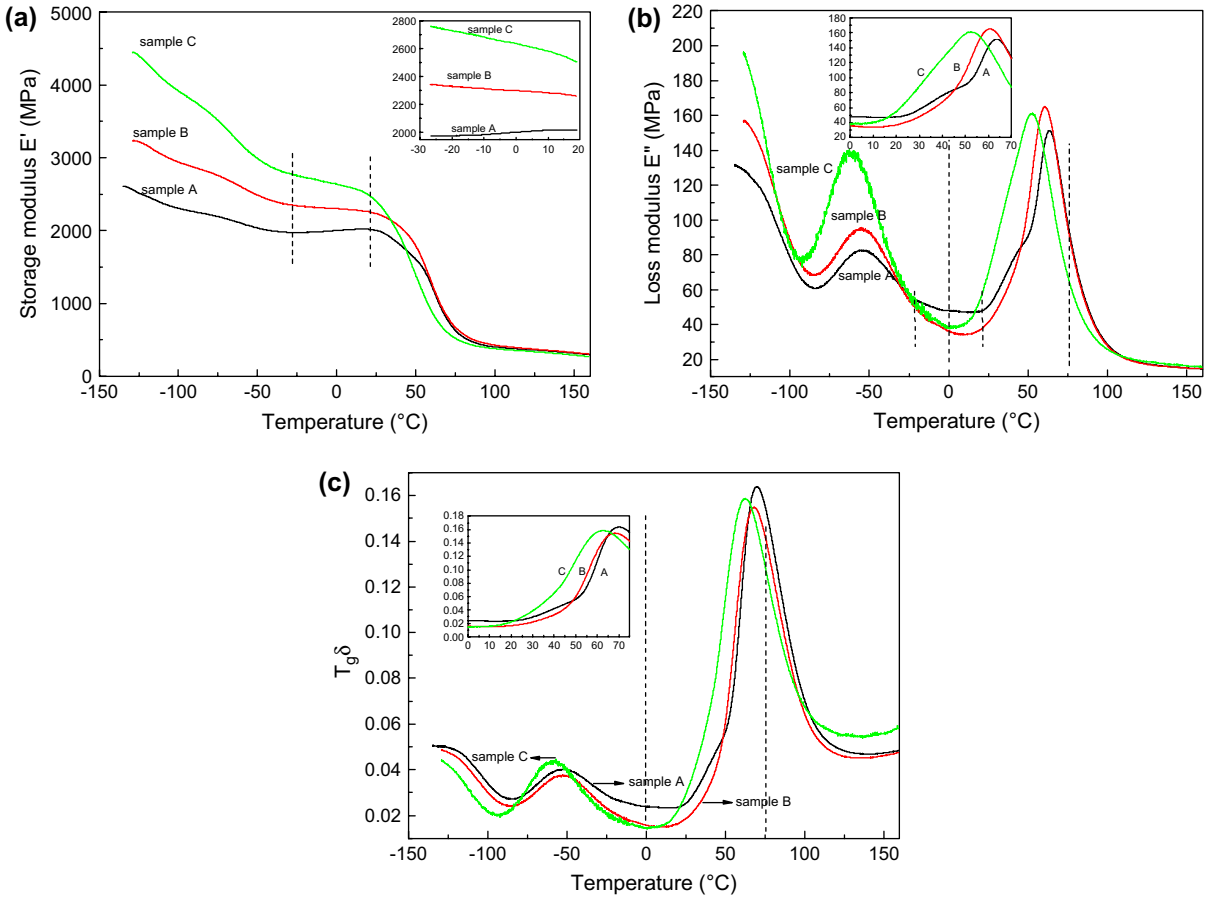

Fig. 11. The dynamic modulus (a) storage modulus; (b) loss modulus; (c) $T_g\delta$ as function of temperature for samples A, B and C.

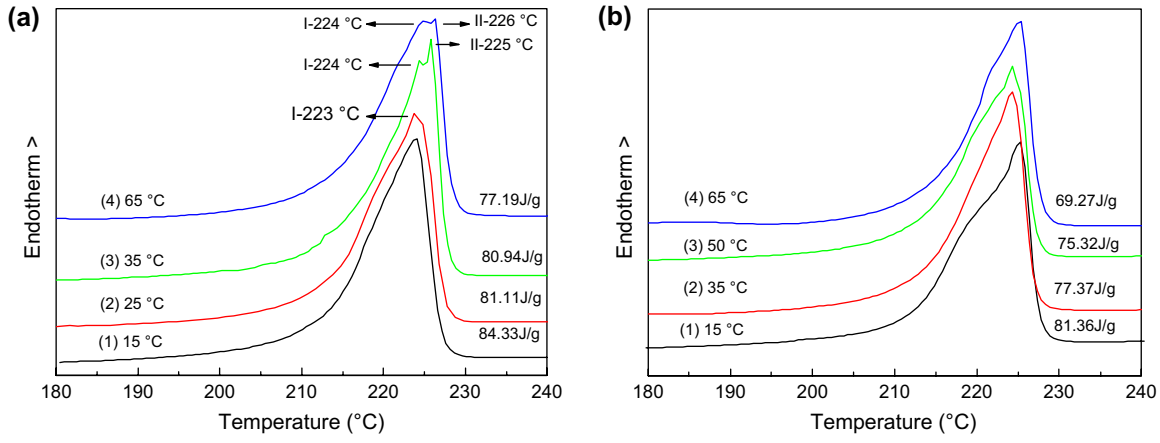

Fig. 12. The DSC melting curves of drawn sample C: (a) $v = 5$ mm/min and (b) $v = 50$ mm/min.

Table 3
The crystallinity of sample C after tensile test at different testing conditions

Strain rate (mm/min)	Temperature (°C)			
	15	25	50	65
5	44.38%	42.69%	42.6%	40.63%
50	42.82%	40.72%	39.64%	36.46%

yielding. Especially, the important role of inter- and intra-link should be taken into account when considering the origin of double yielding of PA6.

5. Conclusions

The major objective of this work is to establish the relation of the dependence of the complex yielding process on the

structural factors and testing conditions. The double yielding really exists in PA6, provided that the definite temperature and strain rate are given, as well as the appropriate initial structure. As the temperature reaches a certain level, the stress–strain curves display a rubber-like deformation and exhibit no evident maximum. It is also revealed that the temperature sensitivity of the first yield stress is nearly linear while the strain rate sensitivity is logarithmic in respect of PA6. Moreover, the temperature and strain rate sensitivity of PA6 change at the temperature in the vicinity of the glass transition temperature of PA6.

Also, the double yielding of PA6 is not only the combination of two thermally activated rate processes depending on temperature and strain rate, but also intimately associated with the initial structure of samples. Some specific structure involving the crystalline and amorphous phases will be in existence in PA6 exhibiting double yielding. The theory of partial melting–recrystallization cannot account fully for the double yielding of PA6. The important role of inter- and intra-link should be taken into account when considering the origin of double yielding of PA6.

Acknowledgements

The authors gratefully acknowledge the financial support of National Natural Science Foundation of China (Grant Nos. 50503014, 50533050), Doctoral Research Foundation granted by the National Ministry of Education, China (Grant No. 20060610029) and the Special Funds for Major Basic Research (Grant No. 2005CB623808).

References

[1] Krausz AS, Eyring H. Deformation kinetics. New York: Wiley Interscience; 1975 [chapter 2].
[2] Zitek P, Zelinger J. J Appl Polym Sci 1970;14:1243–52.
[3] Roetling JA. Polymer 1965;6:311–7.
[4] Bauwens JC. J Polym Sci Part B Polym Phys 1967;5:1145–56.
[5] Vinogradov GV, Dreval VE, Borisenkova EK, Kurbanaliev MK, Shalganova VG. Rheol Acta 1981;20:433–42.
[6] Vinogradov GV, Dreval VE, Borisenkova EK, Kurbanaliev MK, Zabugina MP. J Polym Sci Part B Polym Phys 1986;24:1971–81.
[7] Mahieux CA, Reifsnider KL. Polymer 2001;42:3281–91.
[8] Richeton J, Schlatter G, Vecchio KS, Rémond Y, Ahzi S. Polymer 2005;46:8194–201.
[9] Wang Z, Zhou YX, Mallick PK. Polym Compos 2002;23:858–71.
[10] Seguela R, Rietsch F. J Mater Sci Lett 1990;9:46–7.
[11] Seguela R, Darras O. J Mater Sci 1994;29:5342–52.
[12] Gaucher-Miri V, Seguela R. Macromolecules 1997;30:1158–67.
[13] Brooks NW, Duckett RA, Ward IM. Polymer 1992;33:1872–80.
[14] Lucas JC, Failla MD, Smith FL, Mandelkern L. Polym Eng Sci 1995; 35:1117–23.
[15] Nitta K, Takayanagi M. J Polym Sci Part B Polym Phys 2000;38: 1037–44.
[16] Popli R, Mandelkern L. J Polym Sci Part B Polym Phys 1987;25: 441–83.
[17] Spathis G, Kontou E. J Appl Polym Sci 2004;91:3519–27.
[18] Plaza AR, Ramos E, Manzur A, Olayo R, Escobar A. J Mater Sci 1997; 32:549–54.
[19] Hoashi K, Kawasaki N, Andrews RD. In: Lenz RW, Stein RS, editors. Structure and Properties of Polymer Films. New York: Plenum Press; 1973. p. 283.
[20] Yang W, Shan GF, Wei SP, Li ZM, Xie BH, Yuan XH, et al. Chin Plast 2005;19:22–6.
[21] Shan GF, Yang W, Xie BH, Li ZM, Feng JM, Yang MB. Polym Test 2005;24:704–11.
[22] Shan GF, Yang W, Xie BH, Li ZM, Feng JM, Yang MB. Polym Test 2006;25:452–9.
[23] Shan GF, Yang W, Tang XG, Yang MB, Xie BH, Fu Q. J Polym Sci Part B Polym Phys, in press.
[24] Gurato G, Fichera A, Grandi FZ, Zannetti R, Canal P. Die Makromol Chem 1974;175:953–75.
[25] Campoy I, Gomez MA, Marco C. Polymer 1998;39:6279–88.
[26] Qiu ZM, Wang JH, Zhang QY, Zhang SB, Ding MX, Gao LX. Polymer 2006;47:8444–52.
[27] Ferreiro V, Pennec Y, Seguela R, Coulon G. Polymer 2000;41:1561–9.
[28] Ferreiro V, Depeckera C, Laureynsb J, Coulon G. Polymer 2004;45: 6013–26.
[29] Uribe-Arocha P, Mehler C, Puskas JE, Altstadt V. Polymer 2003;44: 2441–6.
[30] Akkapeddi M. Antec '99 conference proceedings, New York City; May 2–6 1999. p. 1619–22.
[31] McCrum NG, Read BE, Williams G. Anelastic and dielectric effects in polymeric solids. New York: Wiley; 1967. p. 478.
[32] Nitta KH, Takayanagi M. J Polym Sci Part B Polym Phys 1999;37: 357–68.
[33] Balsamo V, Müller AJ. J Mater Sci Lett 1993;12:1457–9.
[34] Butler MF, Donald AM, Ryan AJ. Polymer 1997;38:5521–38.
[35] Butler MF, Donald AM, Ryan AJ. Polymer 1998;39:39–52.
[36] Butler MF, Donald AM, Ryan AJ. Polymer 1998;39:781–92.
[37] Nitta KH. Macromol Symp 2001;170:311–9.